Synthesis of 0.94 Na0.5Bi0.5TiO3 – 0.06 BaTiO3 (NBT-6BT) lead-free piezoelectric powder suitable for aerosol deposition (AD)

Innocent Nomel, Jérôme Lelievre, Laurence Boyer, Olivier Durand-Panteix, Pascal Marchet

▸ To cite this version:

Innocent Nomel, Jérôme Lelievre, Laurence Boyer, Olivier Durand-Panteix, Pascal Marchet. Synthesis of 0.94 Na0.5Bi0.5TiO3 – 0.06 BaTiO3 (NBT-6BT) lead-free piezoelectric powder suitable for aerosol deposition (AD). Ceramics International, 2022, 48 (10), pp.14697-14707. 10.1016/j.ceramint.2022.02.005 . hal-03642105

HAL Id: hal-03642105
https://hal.science/hal-03642105v1

Submitted on 14 Apr 2022

Synthesis of 0.94 $Na_{0.5}Bi_{0.5}TiO_3$ – 0.06 $BaTiO_3$ (NBT-6BT) lead-free piezoelectric powder suitable for aerosol deposition (AD)

Innocent Nomel[1,2], Jérôme Lelievre[1], Laurence Boyer[2], Olivier Durand-Panteix[2], Pascal Marchet[1,*]

[1] Institut de Recherche sur les Céramiques (IRCER),
UMR 7315 CNRS Université de Limoges,
12 rue Atlantis, 87000 Limoges, France

[2] Centre de Transfert de Technologies Céramiques (CTTC),
7 rue Soyouz, 87068 Limoges, France

∗ Corresponding author
Tel: +33 5 87 50 23 73
E-mail address: pascal.marchet@unilim.fr

Abstract

The present work is devoted to the synthesis of 0.94 $(Na_{0.5}Bi_{0.5})TiO_3$ – 0.06 $(BaTiO_3)$ powders by solid-state reaction, suitable for Aerosol Deposition method (AD). The powders were synthetized using Na_2CO_3, Bi_2O_3, $BaCO_3$ and TiO_2. The raw powders were simultaneously milled / mixed by attrition milling in water. Two routes were studied, differing by the order of introduction of the raw materials, for three calcination temperatures. The first route (S1) led to the occurrence of $Bi_2Ti_2O_7$ pyrochlore secondary phase. Attempts to suppress this phase by annealing were unsuccessful. The second route (S2) gave no secondary phase. The large grain size obtained at 950°C and 1050°C are not suitable for sintering or AD. However, the process carried out at 850°C resulted in powders suitable for both sintering and AD method. The ferroelectric and piezoelectric properties of the ceramic samples obtained using these powders are similar to the best-reported ones. Finally, we successfully used these powders for AD.

Keywords: lead-free piezoelectric material, perovskite, piezoelectric properties.

1 Introduction

Currently, piezoelectric ceramic materials are used in a large range of sensors or actuators. We can, for example, mention everyday life devices, such as car parking aid and motor fuel injectors, piezoelectric lighters, piezoelectric microphones and loudspeakers… or industrial and medical ultrasonic applications like non-destructive testing, underwater sonar systems or medical echography… Most of these applications need piezoelectric materials in ceramic form. However, some of them, like piezoelectric sensors or energy-harvesting devices, require thick film shape (1 - 100 µm). Only a few elaboration methods are available for this shaping: screen-printing and aerosol deposition method (AD) [1]. Introduced around year 2000 by Dr J. Akedo [1–3], AD appears now as an interesting emerging process in ceramic technologies, currently co-developed in France by the Center for Transfer of Ceramic Technologies (CTTC) and the Institute of Research on Ceramics (IRCER) since 2010 [4,5]. In

AD, a dry aerosol of ceramic powder, sent by a carrier gas, is projected onto a substrate using a suitable supersonic nozzle. By fragmentation and rearrangement of the ceramic grains, this process leads directly to a consolidated ceramic film [3]. Unlike bulk ceramics, the main advantage of AD is that it does not require sintering. However, one of the key point of this process is the quality of the ceramic powder. Among the necessary conditions, AD use submicronic or micronic powders, generally between 0.8 µm and 10 µm [3]. Therefore, the elaboration of piezoelectric devices by AD associated to our studies requires a controlled powder.

Nowadays, the most widely used piezoelectric materials are $PbZr_{(1-x)}Ti_xO_3$ (PZT) ceramics [6–9]. Indeed, PZT are easy to synthesize and to sinter. Moreover, their electromechanical properties can be easily modulated by doping, allowing a large range of properties and applications, from soft to hard piezoelectric materials. However, due to environmental and health concerns, lead-based materials should be avoided in the future [10,11]. Thus, it is necessary to search for lead-free piezoelectric materials suitable for the substitution of PZT, at least for some applications. The most actively investigated lead-free piezoelectric materials currently considered as potential substitutes for PZT are: (i) Aurivillius phases, such as $Bi_4Ti_3O_{12}$, (ii) barium titanate $BaTiO_3$ (BT) and its derivatives such as (Ba, Ca)(Ti, Zr)O_3 (BCTZ), (iii) alkali-bismuth titanates $(Na_{0.5}Bi_{0.5})TiO_3$ (NBT) or $(K_{0.5}Bi_{0.5})TiO_3$ (KBT) and (iv) alkali niobates (K, Na)NbO_3 (KNN) and their derivatives [12–16]. Currently, none of these materials achieves the performance of PZT. However, despite this handicap, some of these lead-free materials have interesting and sufficient electrical properties for applications.

Among them, sodium bismuth titanate is considered as a potential candidate to the substitution of PZT. NBT is easily synthesized, either by the conventional solid-state route [17–19], by the hydrothermal / solvothermal route [20,21] or by the sol-gel route [22,23]. However, NBT is difficult to pole due to its large coercive field (Ec=7.5 kV/mm [24]). Furthermore, NBT presents some shortcomings like narrow sintering temperature range and high conductivity at room temperature, connected to significant dielectric losses [18,25,26]. These result from the vaporization of bismuth and/or sodium during synthesis and sintering and therefore from the creation of oxygen vacancies which fix the domain walls [27]. The reported piezoelectric properties are d_{33}=78 pC/N, d_{31}=15 pC/N, d_{15}=87 pC/N [19]. Therefore, the applications of pure NBT ceramics are also limited because of moderate values of piezoelectric charge coefficients, despite the interesting value of coupling coefficient k_{33}=0.47 [19].

Fortunately, like other perovskite ferroelectric compounds, the properties of NBT can be easily modified by the formation of solid solutions [18,28–34]. For the (1-x) $(Na_{0.5}Bi_{0.5})TiO_3$ – x($BaTiO_3$) system, hereafter called NBT-xBT, the structural situation is similar to PZT. Indeed, PZT and NBT-xBT are solid solutions between a rhombohedral ($PbZrO_3$ or NBT) and a tetragonal ($PbTiO_3$ or BT) compound. In both case, structural studies evidenced a morphotropic phase boundary (MPB) at the border between these domains, where properties are enhanced. For NBT-xBT, the published results report a MPB composition around x=0.06-0.07 [35–39] where the piezoelectric properties are improved: d_{33}=125 pC/N, d_{31}=40 pC/N, d_{15}=194 pC/N and k_{33}=0.55 [35]. Thus, we retained the NBT-6BT composition for our work on the elaboration of lead-free piezoelectric thick films by AD. Indeed, this material has interesting electrical properties for piezoelectric applications and microelectronics.

The literature reports several methods for synthesizing NBT-6BT powder, in particular the sol-gel route, the hydrothermal route and the solid-state route. Nevertheless, the two first routes are expensive and chemically complicated. Only the solid-state route appears suitable for the synthesis of large amounts of ceramic powders needed for AD. For reasons of cost and simplicity, we retained co-attrition milling of the different raw materials rather than separate milling. Indeed, such process allows a one-step reduction of their grain sizes, with simultaneous homogenization of the mix. For the same reason, we selected water as solvent for attrition because of its low cost and low environmental imprint.

Unfortunately, if many papers devoted to the properties of NBT-6BT are available [35–47], none of them reports a systematic study of the synthesis. Therefore, the aim of the present work is to study the impact of the milling and calcination processes (i) on secondary phases, (ii) on grain size, powder morphology and sintering ability of NBT-6BT powders processed by classical solid-state route and (iii) to test their suitability for the elaboration of films by AD.

2 Materials and methods

2.1 Powder synthesis

Powders of 0.94 $Na_{0.5}Bi_{0.5}TiO_3$ - 0.06 $BaTiO_3$ composition were elaborated through solid-state reaction. The selected precursors are Na_2CO_3 (Aldrich 99.5%), Bi_2O_3 (Alfa-Aesar 99.9995%), $BaCO_3$ (Alfa-Aesar 99.8%) and TiO_2 (Alfa-Aesar 99.8%). The powders were weighed in stoichiometric amount and then homogenized by attrition milling in water, using a polymethacrylate dispersant. The process was carried out at 1000 rpm with 1 mm diameter yttria doped zirconia beads. Two different milling / mixing processes were used, hereafter called S1 and S2, differing in the order of addition of the precursors.

For S1, the idea was to introduce the carbonates first, since Na_2CO_3 have a coarser particle size than the oxides. Barium carbonate is introduced first and treated for 30 min, followed by Na_2CO_3, then milled for the same time. After 1 hour, Bi_2O_3 and TiO_2 are added simultaneously to the mix and the whole is further treated for 2 hours. Thus, the order of introduction is $BaCO_3 \rightarrow Na_2CO_3 \rightarrow [Bi_2O_3 + TiO_2]$.

For S2 route, the idea was to introduce the precursors according to their average particle size (D_{50}) in decreasing order. However, since Na_2CO_3 is soluble in water, we therefore chose to insert chronologically $Bi_2O_3 \rightarrow BaCO_3 \rightarrow [Na_2CO_3 + TiO_2]$. Bi_2O_3 powder is introduced first and attrition milled for 30 min. Then, $BaCO_3$ is introduced and the milling continues for 30 min. After 1 hour milling, the combination $[Na_2CO_3 + TiO_2]$ is added to the mix. The attrition treatment continues for another 2 hours.

The obtained raw powders were dried overnight at 100°C and then calcined for 10 hours at three different temperatures: 850°C, 950°C and 1050°C (heating rate 5°C/min). These values were selected using results obtained from the literature. The aim was to determine the lowest possible temperature to obtain suitable powders, in order to limit the grain growth, the bismuth evaporation and the energetic cost. After synthesis and characterization, we also examined the effect of annealing on the powders for 1 hour at the same temperature, in order to estimate the influence of such thermal treatment on phase purity and grain growth. Before annealing, the powders were attrition-milled for one hour at 1000 rpm in order to decrease the grain size and the amount of agglomerates.

2.2 Characterization techniques

The grain size distribution of the powders was determined using a laser particle size analyzer (Horiba LA 950 V2 Pratica). The measurements were carried out in water. The grain size distribution was extracted from the measurements considering the Fraunhofer approximations. From the literature, the refractive index of NBT-6BT is estimated to be between 2.35 and 2.55. The same device was used to follow the grain size evolution during attrition milling and also after synthesis and annealing of the powders. D_{10}, D_{50} and D_{90} are the mean diameters associated respectively to 10%, 50% and 90% of the statistical population.

The morphology of the powders was examined by scanning electron microscopy (SEM, LEO 1530 VP). The structural characterization of the powders and phase identification was performed by X-ray diffraction (XRD), using a θ / 2θ diffractometer (Bruker D8) with Cu $K\alpha_1$ wavelength (λ = 1.5406 Å). The crystalline phases were determined from XRD patterns recorded for 60 min, for 2θ values ranging from 20° to 80° with a step of 0.02°.

The density of the powders was determined at room temperature using a pycnometer (Accupyc II 1340, Micrometrics). For the best obtained powders, dilatometric measurements were performed up to 1160°C (5 min dwell time), with 5°C/min heating and cooling rate (Setaram, TMA setsys evo 1600).

The ferroelectric cycles of the ceramic samples were obtained at room temperature using the aixACCT device fitted with piezo sample holder unit (PSHU, Aixacct, Germany). The converse d_{33}* piezoelectric coefficient was determined using the slope of the piezoelectric strain cycle. The dielectric properties and resonance curves of the ceramic samples after poling were measured using an impedance meter (Agilent 4294A) between 10 kHz and 5 MHz. The piezoelectric coupling coefficients k_p and k_t were calculated by the IEEE standard method using the resonance / antiresonance frequencies determined by impedance curves.

3 Results and discussions

3.1 Characterization of the precursors

The particle size measurements and the morphology of raw precursors obtained by SEM are represented in Fig. 1. The results evidence that Na_2CO_3 present very large grain size (484 µm) with single mode distribution. For $BaCO_3$, the grains present irregular morphology with a mean diameter around 1.6 µm. Bi_2O_3 powder is associated to a bimodal distribution, showing both faceted large grains (3.3 µm) and irregular small particles (0.3 - 0.4 µm). Finally, TiO_2 grains are smaller (0.4 µm) than all the other raw materials. The large difference of the measured grain size (D_{50}) confirms the requirement of milling in order to decrease grain size and thus increase reactivity before calcination.

3.2 Processing of the NBT-6BT mixture before calcination

3.2.1 Attrition milling and evolution of particle size during attrition-milling

As mentioned hereabove, the synthesis route S1 differs from S2 in the order of addition of the precursors in the attrition system. During the process, samples were drawn from the mix every 15 min, in order to measure the grain size distribution. Each time a precursor is added, a sample was drawn just before the addition (T0 + 30, T1 + 30) and just after (T1, T2). The grain size evolution for S1 and S2 routes (D_{10}, D_{50} and D_{90}) is presented in Fig. 2 and Fig. 3. For S1, the results evidence an increase of the grain size after the introduction of Na_2CO_3 (D_{50} and D_{90}). Since Na_2CO_3 presents high solubility in water while $BaCO_3$ is only weakly soluble, this grain size increase can be attributed to the precipitation of sodium carbonate, probably onto the surface of barium carbonate. Thus, this phenomenon is detrimental to the chemical homogeneity of the powder. We did not observed a similar phenomenon for S2 after the introduction of [Na_2CO_3 + TiO_2]. Therefore, S2 route will probably induce better chemical homogeneity than S1.

However, for both S1 and S2 routes and after 3 hours of attrition milling, an average grain size (D_{50}) around 1 µm is obtained. The large particles observed before milling, especially for Na_2CO_3 (D_{50} around 480 µm) are no more present. At this stage of the powder processing, there is no obvious difference in grain size between the S1 and S2 routes and the D_{50} is similar.

This result evidences that both routes allow a reduction in the grain size toward the desired value, around 1 µm, as expected from attrition milling.

3.2.2 XRD and densities of calcined and annealed powders

The XRD patterns of the powders calcined at 850°C, 950°C and 1050°C for 10h are presented in Fig. 4, together with the patterns of the 1 hour annealed powders. As expected, all XRD patterns reveal a perovskite phase, similar to the one reported for NBT-6BT (PDF4 00-063-0299). We also detected a pyrochlore $Bi_2Ti_2O_7$ secondary phase in different amounts, depending of the processing parameters. For S1 route, the amount of pyrochlore phase is large after the calcination at 850°C and decrease with increasing synthesis temperature (Fig 4.a). Further annealing at the same temperature for one hour did not succeed in the elimination of this secondary phase (Fig 4.b). This result confirms that S1 route did not succeed in the chemical homogenization of the precursors. For S2 route, we obtained only a minor amount of $Bi_2Ti_2O_7$ secondary phase after the calcination at 850°C, without secondary phase for the other temperatures (Fig 4.c). A one hour annealing easily eliminates this secondary phase (Fig 4.d).

The densities of powders resulting from S1 and S2 routes are reported in table 1. The relative values are only indicatives and were calculated considering a theoretical density of 5.95±0.01 g/cm^3 (reference file: PDF4 00-063-0299). Globally, the densities are higher for S1 route (5.86 – 5.96) than for S2 route (5.66 – 5.77). This reflects the occurrence of pyrochlore secondary phase, since $Bi_2Ti_2O_7$ presents a higher density of 7.43 g/cm^3 (ISCD #99437) than NBT-6BT. For S1 route, the densities globally increase while increasing calcination temperature (5.87 $\rightarrow$ 5.94). The annealing globally does not change the density values, apart at 1050°C (5.94 $\rightarrow$ 5.86). This last result probably comes from bismuth evaporation, since bismuth volatility at high temperature is well known for Bi-containing compounds. For S2, the obtained densities (5.67) are lower than for S1. This result agrees well with the absence of secondary phase observed by XRD (only a small amount of this phase was detected at 850°C/10h). The measurements reveal an almost constant density (5.67) whatever the calcination temperature. Annealing increases the density values, probably indicating a better crystalline order after this further thermal treatment. Contrary to S1, annealing performed at 1050°C improves the density (5.67 $\rightarrow$ 5.72), probably indicating that bismuth losses are higher for the pyrochlore phase than for perovskite phase.

To sum up, S2 route leads to better results than S1, since no secondary phase appears from 950°C. A short annealing (1h) slightly increases the density, indicating a better crystalline order after annealing. Therefore, these results evidence that S2 route is favorable for obtaining the expected perovskite phase. Study of grain size and morphology will allow determination of the best calcination temperature.

3.2.3 Grain size and grain morphology of the calcined and annealed powders

Figure 5 represents the particle size distribution of the powders after calcination and annealing for both S1 and S2 routes and Figure 6 the corresponding SEM pictures. The analyses reveal a multimodal distribution of grain size for all samples. We remind that before annealing, the powders were attrition milled for one hour at 1000 rpm in order to decrease the amount of agglomerates.

The measurements of S1 powders (Fig. 5.a.) present micrometer-sized particles (1.2 - 1.5 µm) together with larger grains (30 - 45 µm) and very large ones assimilated to agglomerates (100 – 200 µm). The syntheses at the two lowest calcination temperatures, 850°C and 950°C, lead to a high volume fraction of fine particles. The synthesis at 1050°C gives an equivalent volume of fine particles and larger grains. The corresponding SEM pictures

(Fig.6 a, b, c) confirm the particle distribution results. Indeed, the powder synthetized at 850C°/10h presents small grains, around 1 µm, associated to larger agglomerates composed of these grains. For 950°C, the elementary particles have a size with the same order of magnitude (1 µm), but their agglomeration degree increases. For the powders processed at 1050°C, the elementary grains are a little bit larger. Moreover, the grains are not only agglomerated, but a large degree of coalescence is noticed. In addition, we observe agglomerated round-shaped very large grains. This result clearly indicates that sintering has begun for this temperature (1050°C) and to some lower extent for 950°C.

The grain size of S1 annealed powders (Fig. 5.b) still presents a bimodal distribution. For 850°C, two populations are observed (0.45 and 1.5 µm), in agreement with the SEM picture (Fig. 6.d). For 950°C, most of the grain are measured around 1.5 µm, composed of smaller particles partly agglomerated (Fig. 6.e). Logically, for 1050°C (Fig. 6.f), the intermediate milling did not succeed in breaking the large and partly sintered grains observed after calcination.

For S2, the grain-size distribution curves (Fig. 5.c) present particles around 1 µm for calcinations at 850°C and 950°C. For 1050°C, the smallest population is around 13 µm. For all the temperatures, another population larger than 30 µm is also observable. For 850°C (Fig. 6.g), the grain size observed by SEM is around 1 µm, with only low agglomeration degree. For 950°C (Fig. 6.h) and 1050°C (Fig. 6.i), the increasing temperature induces an increase of the coalescence degree of the elementary grains. The bridging between these grains changes and bottleneck grain boundaries appear, as usually reported in the sintering process.

For the S2 sample annealed at 850°C (Fig. 5.d.), the short milling before thermal treatment allowed to reduce the grain size, since a new population is observed around 0.3 µm, while the second one remains around micrometer size (2.6 µm). The population at 77 µm is attributed to agglomerates, according to SEM picture (Fig. 6.j). For 950°C and 1050°C (Fig. 5.d.), the annealing lead to an increase of the grain size with two populations, at 13 µm and ~100 µm for 950°C, and around ~80 µm and 200 µm for 1050°C. These measurements agree well with the SEM pictures (Fig. 6.k and 6.l) which also show that annealing increases the coalescence degree compared to unannealed samples.

To summarize, the results of both grain size measurements and SEM pictures evidence that synthesis at 850°C leads to a grain size around 1µm. The intermediate milling followed by annealing keeps the same grain size, with low degree of agglomeration. As the AD process requires micronic powders, the process with 850°C calcination without annealing, seems to be the most appropriate for powders suitable for the deposition tests. For 950°C and 1050°C, the increase of the temperature lead to larger grain size, with a coalescence degree more and more pronounced with higher temperatures. The SEM pictures evidence bottleneck grain boundaries between rounded grains, showing that sintering has already begun. In addition, the rounded grain shape could suggest the occurrence of a liquid phase. Indeed, the TiO_2 - Bi_2O_3 phase diagram indicates an eutectic point at 835°C for 97 mol% Bi_2O_3. Thus, it is likely that a transient liquid phase occurs during calcination.

3.3 Dilatometric study of the powders and sintering

As only the S2 route gave the NBT-6BT perovskite compound without secondary phase, dilatometric measurements were performed for the S2 powders calcined at 850°C, 950°C and 1050°C (Fig. 7). For these powders, the shrinkage associated to sintering begins around 950°C. Then, its rate increases around 1000°C, giving a maximum rate around 1100°C. However, the final shrinkage is different and depends on the calcination temperature of the powder. The final values are 18.8%, 15.9% and 7.2% respectively for 850°C, 950°C and 1050°C samples. They confirm the previous conclusion obtained by characterizations of powders. Indeed, since shrinkage begin around 950°C (Fig. 7), sintering already occurred during calcination for the 950°C/10h and 1050°C powders. Furthermore, for the 1050°C powder, the calcination led to rounded and large grains (10 - 100 µm), with high degree of grain coalescence. Thus, this powder is unsuitable for sintering, as demonstrated by the low value of final shrinkage (7.2%). The coalescence degree of 950°C powders is lower, leading to a higher final shrinkage (15.9%). However, both 950°C and 1050°C powders give lower sintering results than the 850°C ones, as supposed with the previous characterizations. Therefore, only 850°C powders appear to be suitable for sintering, with a final shrinkage value compatible with ceramic densification (18.8%).

3.4 Electrical properties of ceramics

In order to evaluate the ferroelectric/piezoelectric properties of ceramics obtained by these powders, ceramic samples were sintered using the S2 850°C/10h powder. Before sintering, the powder was treated by planetary milling (300 rpm, 2x15 min). The powder was then pressed into pellets of 25 mm in diameter and around 1 mm in thickness with a uniaxial pressure of 125 MPa. The sintering was then performed at 1150°C for 10 h. After surface polishing, silver was deposited on the pellets by sputtering. The poling of the ceramic samples was performed in silicon oil at 80°C for 4 kV/mm electric field.

Figure 8 (a) shows a typical ferroelectric / piezoelectric cycle hysteresis loop for the NBT-6BT pellet. The remnant polarization (Pr) and the coercive electric field (Ec) obtained from the P(E) hysteresis loops are 53.5 $\mu C/cm^2$ and 2.5 kV/mm, respectively. The Pr value is slightly higher than reported values, Ec≈30-40 $\mu C.cm^{-2}$ [48–50], while Ec value have the same order of magnitude Pr≈3 $kV.mm^{-1}$ [48,49]. Thus, these measured values are characteristics of a well-prepared powder and a well-densified ceramic. However, the polarization loop (Fig. 8 a) appears “rounded” for high fields. The saturation polarization is not fully reached, thus indicating a lossy behavior. This could be due to chemical defects induced by sintering, like oxygen vacancies. Indeed, the Bi-based materials are known as highly sensitive to bismuth losses during calcination and sintering. They induce oxygen vacancies which result in leakage current and pinning of the domain walls, associated to difficulty in poling process [51–53]. Further experiments are in progress in order to improve the sintering and obtain better polarization loops.

Figure 8 (b) represents the S(E) strain – field unipolar response of the NBT-6BT pellet. A maximum strain of 0.11% was obtained for a 2.6 $kV.mm^{-1}$ field (2500 V). This value makes them similar to the strain of ≈0.1% obtained for PZT ceramic materials [54] and for undoped NBT-BT [55,56]. The d_{33}* converse piezoelectric coefficient, obtained from the piezoelectric cycle, is 358 $pm.V^{-1}$, very close to the best-reported values for undoped NBT-6BT ceramics (240-380 $pm.V^{-1}$) [55,56].

The measurements of the impedance curves around the resonances associated radial mode and thickness mode allowed the calculation of the coupling coefficients k_p and k_t. The calculated values are k_p=0.22 and k_t=0.37. These results agree well with the ones previously reported for NBT-6BT ceramic samples: k_p=0.29 and k_t=0.40 [35]. These results confirm the high quality of the powder obtain by the S2 route, which appears thus suitable for AD.

3.5 Aerosol Deposition tests

Finally, we used the obtained powders for AD tests, using the apparatus reported in a previous paper [4]. For these purpose, we retained a metallic Kovar substrate (thickness 0.125

mm) for their use in the future elaboration of piezoelectric devices. The XRD pattern of the NBT-6BT film is presented in Fig.9. As a matter of comparison, the XRD patterns of the powder and of the kovar substrate are also presented, as well as the JCPDS card of NBT-6BT. The main XRD peak of NBT-6BT, observed around 32.5°, indicates that the film deposited by AD has the same perovskite structure as the powder. However, the XRD pattern of the AD film presents low diffracted intensity compared to that of the powder, together with a widening of the diffraction peaks. These phenomena clearly indicate a low grain size for the AD film compared to the powder. There is indeed a reduction in the grain size of the film linked to their distortion during deposition. The SEM top view (Fig. 9 b) evidences a rough surface, with occurrence of craters, one of the characteristic of the AD films. The SEM cross section obtained for a film prepared by Focused Ion Beam (Fig. 9. b) reveals a thickness of 38 µm. Despite the presence of micro porosities, the film presents a high density. These results indicate that we successfully obtained a NBT-6BT thick film by AD using our powder. The study of the properties of such films is under investigation and will be reported latter.

4 Conclusion

The aim of the present work was the study of the synthesis process of ceramic powders of lead-free piezoelectric material, devoted to the elaboration of piezoelectric thick films by aerosol deposition method (AD). For this purpose, we selected the 0.94 $(Na_{0.5}Bi_{0.5})TiO_3$ – 0.06 $(BaTiO_3)$ (NBT-6BT) lead-free composition because of its piezoelectric properties. Since AD requires large batches of powder, we selected the classical solid-state route for the synthesis. Indeed, this method is the easiest and cheapest one in order to obtain large quantities of powder (100–500 g). The selected precursors are Na_2CO_3, Bi_2O_3, $BaCO_3$ and TiO_2 because of their low cost compared to precursors required by other methods.

Before calcination, stoichiometric amounts of powders were homogenized / milled by attrition milling. For the same reason of simplicity and cost, we retained a one-step milling in water, rather than separate milling of the precursors and a more expensive solvent. We studied two different routes for the milling, which differ by the order of introduction of the precursors. The best results were obtained using the S2 route, which corresponds chronologically to $Bi_2O_3 \rightarrow BaCO_3 \rightarrow [Na_2CO_3 + TiO_2]$. Indeed, this route gave better chemical homogeneity of the precursors mix before calcination. Moreover, it avoids the occurrence of the $Bi_2Ti_2O_7$ pyrochlore secondary phase (at 950°C and 1050°C) or limits it at 850°C.

These powders were calcined at three different temperatures for 10h: 850°C, 950°C and 1050°C. We also studied the influence of a post-calcination milling followed by a short annealing (1h) at the same temperature, in order to reduce the amount of secondary phase. The results evidenced that this elimination cannot be obtained when the chemical homogeneity is poor before calcination (S1 route) whereas this post treatment is efficient for S2 powders. The calcination and annealing at the highest temperature, 950°C/10h and 1050°C/10h, led to large grain size, with high coalescence of the grains. As demonstrated by the dilatometric measurements, this phenomenon comes from the pre-sintering of the NBT-6BT powder during calcination. Indeed, the shrinkage starts around 950°C with a maximum rate around 1100°C. Therefore, the best powders are the ones calcined at 850°C, lower that the starting sintering temperature.

In order to test the ability of the powders for ceramic elaboration and their ability for AD method, ceramic samples were sintered using these powders. The results of the ferroelectric / piezoelectric measurements, d_{33}*=358 pm/V, k_p=0.22 and k_t=0.37 are similar to the best reported values for NBT-6BT. Because of these electrical properties, and since the grain size of this powder is around 1 µm, this synthesis process appears suitable for its use in aerosol deposition. Finally, we used these powders for AD test and obtained successfully NBT-6BT dense films with a thickness of tens of micrometers. The properties of these films are under investigation and will be reported latter.

Acknowledgments:

This work was supported by Region Nouvelle Aquitaine [project PICORE 2018-1R10112] which funded the postdoctoral position of J. Lelievre

References

[1] J. Akedo, J.R. Ryu, Aerosol Deposition (AD) and Its Applications for Piezoelectric Devices, in: Advanced Piezoelectric Materials, 2nd edition, Woodhead Publishing in Materials, 2017.

[2] J. Akedo, M. Ichiki, K. Kikuchi, R. . Maeda, Fabrication of three dimensional micro structure composed of different materials using excimer laser ablation and jet molding, Proceedings of the 1997 IEEE 10th Annual International Workshop on Micro Electro Mechanical Systems. (1997) 135–140.

[3] J. Akedo, Chapter 10.5 - Aerosol Deposition Method for Room-Temperature Ceramic Coating and Its Applications, in: S. Somiya (Ed.), Handbook of Advanced Ceramics (Second Edition), Academic Press, Oxford, 2013: pp. 847–860. https://doi.org/10.1016/B978-0-12-385469-8.00046-0.

[4] M.A. Piechowiak, J. Henon, O. Durand-Panteix, G. Etchegoyen, V. Coudert, P. Marchet, F. Rossignol, Growth of dense Ti_3SiC_2 MAX phase films elaborated at room temperature by aerosol deposition method, J. Eur. Ceram. Soc. 34 (2014) 1063–1072. https://doi.org/10.1016/j.jeurceramsoc.2013.11.019.

[5] J. Henon, M.A. Piechowiak, O. Durand-Panteix, G. Etchegoyen, O. Masson, C. Dublanche-Tixier, P. Marchet, B. Lucas, F. Rossignol, Dense and highly textured coatings obtained by aerosol deposition method from Ti_3SiC_2 powder: Comparison to a dense material sintered by Spark Plasma Sintering, J. Eur. Ceram. Soc. 35 (2015) 1179–1189. https://doi.org/10.1016/j.jeurceramsoc.2014.10.012.

[6] B. Jaffe & al, Piezoelectric Ceramics, Academic, New York, 1971, 1971.

[7] J.W. Waanders, Piezoelectric Ceramics-Properties and Applications, Philips Components, Eindhoven, 1991.

[8] A.J. Moulson, Electroceramics: Materials, Properties and Applications, John Wiley & Sons Ltd., New York, 2003.

[9] N. Setter, Piezoelectric Materials and Devices, EPFL Swiss Federal Institute of Technology, Lausanne, 2005.

[10] Directive 2002/95/EC of the European Parliament and of the Council of 27 January 2003 on the restriction of the use of certain hazardous substances in electrical and electronic equipment, 2003. http://data.europa.eu/eli/dir/2002/95/oj/eng (accessed December 1, 2020).

[11] RoHS directive, Directive 2011/65/EU of the European Parliament and of the Council of 8 June 2011 on the restriction of the use of certain hazardous substances in electrical and electronic equipment (RoHS), Official Journal of the European Union. L174 (2011) 88–110.

[12] M.D. Maeder, D. Damjanovic, N. Setter, Lead Free Piezoelectric Materials, J. Electroceram. 13 (2004) 385–392. https://doi.org/10.1007/s10832-004-5130-y.

[13] T. Takenaka, H. Nagata, Y. Hiruma, Y. Yoshii, K. Matumoto, Lead-free piezoelectric ceramics based on perovskite structures, J. Electroceram. 19 (2007) 259–265. https://doi.org/10.1007/s10832-007-9035-4.

[14] S. Zhang, R. Xia, T.R. Shrout, Lead-free piezoelectric ceramics vs. PZT?, J. Electroceram. 19 (2007) 251–257. https://doi.org/10.1007/s10832-007-9056-z.

[15] P.K. Panda, Review: environmental friendly lead-free piezoelectric materials, J. Mater. Sci. 44 (2009) 5049–5062. https://doi.org/10.1007/s10853-009-3643-0.

[16] J. Rödel, W. Jo, K.T.P. Seifert, E.-M. Anton, T. Granzow, D. Damjanovic, Perspective on the Development of Lead-free Piezoceramics, J. Am. Ceram. Soc. 92 (2009) 1153–1177. https://doi.org/10.1111/j.1551-2916.2009.03061.x.

[17] O. Elkechai, P. Marchet, P. Thomas, M. Manier, J.-P. Mercurio, Structural and dielectric study of the $Na_{0.5}Bi_{0.5}TiO_3$–$PbTiO_3$ and $K_{0.5}Bi_{0.5}TiO_3$–$PbTiO_3$ systems, J. Mater. Chem. 7 (1997) 91–97. https://doi.org/10.1039/A602148D.

[18] S. Said, J.-P. Mercurio, Relaxor behaviour of low lead and lead free ferroelectric ceramics of the $Na_{0.5}Bi_{0.5}TiO_3$-$PbTiO_3$ and $Na_{0.5}Bi_{0.5}TiO_3$–$K_{0.5}Bi_{0.5}TiO_3$ systems, J. Eur. Ceram. Soc. 21 (2001) 1333–1336. https://doi.org/10.1016/S0955-2219(01)00012-7.

[19] Y. Hiruma, H. Nagata, T. Takenaka, Thermal depoling process and piezoelectric properties of bismuth sodium titanate ceramics, J. Appl. Phys. 105 (2009). https://doi.org/10.1063/1.3115409.

[20] Y. Liu, Y. Lu, S. Dai, Hydrothermal synthesis of monosized $Bi_{0.5}Na_{0.5}TiO_3$ spherical particles under low alkaline solution concentration, J. Alloy. Compd. 484 (2009) 801–805. https://doi.org/10.1016/j.jallcom.2009.05.033.

[21] T. Lu, J. Dai, J. Tian, W. Song, X. Liu, L. Lai, H. Chu, X. Huang, X. Liu, Synthesis of $Na_{0.5}Bi_{0.5}TiO_3$ powders through hydrothermal method, J. Alloy. Compd. 490 (2010) 232–235. https://doi.org/10.1016/j.jallcom.2009.09.144.

[22] F. Rémondière, B. Malič, M. Kosec, J.-P. Mercurio, Synthesis and crystallization pathway of $Na_{0.5}Bi_{0.5}TiO_3$ thin film obtained by a modified sol-gel route, J. Eur. Ceram. Soc. 27 (2007) 4363–4366. https://doi.org/10.1016/j.jeurceramsoc.2007.02.208.

[23] T. Šetinc, M. Spreitzer, S. Kunej, J. Kovač, D. Suvorov, Temperature stable dielectric behavior of sol-gel derived compositionally graded $SrTiO_3$ / $Na_{0.5}Bi_{0.5}TiO_3$ / $SrTiO_3$ thin films, J. Am. Ceram. Soc. 96 (2013) 3511–3517. https://doi.org/10.1111/jace.12519.

[24] M. Spreitzer, M. Valant, D. Suvorov, Sodium deficiency in $Na_{0.5}Bi_{0.5}TiO_3$, J. Mater. Chem. 17 (2007) 185–192. https://doi.org/10.1039/b609606a.

[25] H. Nagata, T. Takenaka, Additive effects on electrical properties of $(Bi_{1/2}Na_{1/2})TiO_3$ ferroelectric ceramics, J. Eur. Ceram. Soc. 21 (2001) 1299–1302. https://doi.org/10.1016/S0955-2219(01)00005-X.

[26] Y. Lin, S. Zhao, N. Cai, J. Wu, X. Zhou, C.W. Nan, Effects of doping Eu_2O_3 on the phase transformation and piezoelectric properties of $Na_{0.5}Bi_{0.5}TiO_3$-based ceramics, Mater. Sci. Eng. B-Solid State Mater. Adv. Technol. 99 (2003) 449–452. https://doi.org/10.1016/S0921-5107(02)00465-8.

[27] H. Nagata, Electrical properties and tracer diffusion of oxygen in some Bi-based lead-free piezoelectric ceramics, J. Ceram. Soc. Jpn. 116 (2008) 271–277. https://doi.org/10.2109/jcersj2.116.271.

[28] K. Sakata, Y. Masuda, Ferroelectric and Antiferroelectric Properties of $(Na_{0.5}Bi_{0.5})TiO_3$-$SrTiO_3$ Solid Solution Ceramics, Ferroelectrics 7 (1974) 347–349. https://doi.org/10.1080/00150197408238042.

[29] T. Takenaka, K. Sakata, K. Toda, Acoustic wave characteristics of lead-free $(Bi_{1/2}Na_{1/2})_{0.99}Ca_{0.01}TiO_3$ piezoelectric ceramic, Jpn. J. Appl. Phys. 28 (1989) 59–62. https://doi.org/10.7567/JJAPS.28S2.59.

[30] T. Takenaka, Y. Naitou, K. Sakata, Piezoelectric ceramics of $(Bi_{1/2}Na_{1/2})TiO_3$-$PbTiO_3$-$BaTiO_3$ system, Electrical Engineering in Japan. 112 (1992) 92–101. https://doi.org/10.1002/eej.4391120709.

[31] O. Elkechai, M. Manier, J.P. Mercurio, $Na_{0.5}Bi_{0.5}TiO_3$-$K_{0.5}Bi_{0.5}TiO_3$ (NBT-KBT) system: A structural and electrical study, Phys. Status Solidi A-Appl. Res. 157 (1996) 499–506. https://doi.org/10.1002/pssa.2211570234.

[32] H. Nagata, T. Takenaka, Lead-free piezoelectric ceramics of $(Bi_{1/2}Na_{1/2})TiO_3$-$1/2(Bi_2O_3{\cdot}Sc_2O_3)$ system, Jpn. J. Appl. Phys. Part 1 - Regul. Pap. Short Notes Rev. Pap. 36 (1997) 6055–6057. https://doi.org/10.1143/jjap.36.6055.

[33] P. Marchet, E. Boucher, V. Dorcet, J.P. Mercurio, Dielectric properties of some low-lead or lead-free perovskite-derived materials: $Na_{0.5}Bi_{0.5}TiO_3$–$PbZrO_3$, $Na_{0.5}Bi_{0.5}TiO_3$–$BiScO_3$ and $Na_{0.5}Bi_{0.5}TiO_3$–$BiFeO_3$ ceramics, J. Eur. Ceram. Soc. 26 (2006) 3037–3041. https://doi.org/10.1016/j.jeurceramsoc.2006.02.024.

[34] V. Dorcet, P. Marchet, G. Trolliard, Structural and dielectric studies of the $Na_{0.5}Bi_{0.5}TiO_3$–$BiFeO_3$ system, J. Eur. Ceram. Soc. 27 (2007) 4371–4374. https://doi.org/10.1016/j.jeurceramsoc.2007.02.173.

[35] T. Takenaka, K.-I. Maruyama, K. Sakata, $(Bi_{1/2}Na_{1/2})TiO_3$-$BaTiO_3$ system for lead-free piezoelectric ceramics, Jpn. J. Appl. Phys. 30 (1991) 2236–2239. https://doi.org/10.1143/JJAP.30.2236.

[36] B.-J. Chu, D.-R. Chen, G.-R. Li, Q.-R. Yin, Electrical properties of $Na_{1/2}Bi_{1/2}TiO_3$-$BaTiO_3$ ceramics, J. Eur. Ceram. Soc. 22 (2002) 2115–2121. https://doi.org/10.1016/S0955-2219(02)00027-4.

[37] J.-R. Gomah-Pettry, S. Saïd, P. Marchet, J.-P. Mercurio, Sodium-bismuth titanate based lead-free ferroelectric materials, J. Eur. Ceram. Soc. 24 (2004) 1165–1169. https://doi.org/10.1016/S0955-2219(03)00473-4.

[38] Y. Qu, D. Shan, J. Song, Effect of A-site substitution on crystal component and dielectric properties in $Bi_{0.5}Na_{0.5}TiO_3$ ceramics, Mater. Sci. Eng. B-Solid State Mater. Adv. Technol. 121 (2005) 148–151. https://doi.org/10.1016/j.mseb.2005.03.023.

[39] R. Ranjan, A. Dviwedi, Structure and dielectric properties of $(Na_{0.50}Bi_{0.50})_{1-x}Ba_xTiO_3$: $0 \leq x \leq 0.10$, Solid State Commun. 135 (2005) 394–399. https://doi.org/10.1016/j.ssc.2005.03.053.

[40] M. Chen, Q. Xu, B.H. Kim, B.K. Ahn, J.H. Ko, W.J. Kang, O.J. Nam, Structure and electrical properties of $(Na_{0.5}Bi_{0.5})_{1-x}Ba_xTiO_3$ piezoelectric ceramics, J. Eur. Ceram. Soc. 28 (2008) 843–849. https://doi.org/10.1016/j.jeurceramsoc.2007.08.007.

[41] F. Cordero, F. Craciun, F. Trequattrini, E. Mercadelli, C. Galassi, Phase transitions and phase diagram of the ferroelectric perovskite $(Na_{0.5}Bi_{0.5})_{1-x}Ba_xTiO_3$ by anelastic and dielectric measurements, Physical Review B - Condensed Matter and Materials Physics. 81 (2010). https://doi.org/10.1103/PhysRevB.81.144124.

[42] C. Ma, X. Tan, Phase diagram of unpoled lead-free $(1-x)(Bi_{1/2}Na_{1/2})TiO_3$-$xBaTiO_3$ ceramics, Solid State Communications. 150 (2010) 1497–1500. https://doi.org/10.1016/j.ssc.2010.06.006.

[43] C. Ma, X. Tan, E. Dul'Kin, M. Roth, Domain structure-dielectric property relationship in lead-free (1-x) $(Bi_{1/2}Na_{1/2})TiO_3$- x $BaTiO_3$ ceramics, J. Appl. Phys. 108 (2010). https://doi.org/10.1063/1.3514093.

[44] W. Jo, J.E. Daniels, J.L. Jones, X. Tan, P.A. Thomas, D. Damjanovic, J. Rödel, Evolving morphotropic phase boundary in lead-free $(Bi_{1/2}Na_{1/2})TiO_3$-$BaTiO_3$ piezoceramics, J. Appl. Phys. 109 (2011). https://doi.org/10.1063/1.3530737.

[45] F. Craciun, C. Galassi, R. Birjega, Electric-field-induced and spontaneous relaxor-ferroelectric phase transitions in $(Na_{1/2}Bi_{1/2})_{1-x}Ba_xTiO_3$, J. Appl. Phys. 112 (2012). https://doi.org/10.1063/1.4770326.

[46] C. Ma, H. Guo, S.P. Beckman, X. Tan, Creation and destruction of morphotropic phase boundaries through electrical poling: A case study of lead-free $(Bi_{1/2}Na_{1/2})TiO_3$-$BaTiO_3$ piezoelectrics, Phys. Rev. Lett. 109 (2012). https://doi.org/10.1103/PhysRevLett.109.107602.

[47] L.E. Fuentes-Cobas, L. Pardo, M.E. Montero-Cabrera, J.R. Plaisier, A. García, K. Brebøl, E. Mercadelli, C. Galassi, The $0.96(Bi_{0.5}Na_{0.5})TiO_3$ - $0.04BaTiO_3$ crystal structure: A high-Q, high-counting statistics synchrotron diffraction analysis, Crystal Research and Technology. 49 (2014) 190–194. https://doi.org/10.1002/crat.201300433.

[48] X. Wang, H.L.-W. Chan, C.-L. Choy, Piezoelectric and dielectric properties of CeO_2-added $(Bi_{0.5}Na_{0.5})_{0.94}Ba_{0.06}TiO_3$ lead-free ceramics, Solid State Commun. 125 (2003) 395–399. https://doi.org/10.1016/S0038-1098(02)00816-5.

[49] A. Prado, L. Ramajo, J. Camargo, A. del Campo, P. Öchsner, F. Rubio-Marcos, M. Castro, Stabilization of the morphotropic phase boundary in $(1 - x)Bi_{0.5}Na_{0.5}TiO_3$–$xBaTiO_3$ ceramics through two alternative synthesis pathways, J Mater Sci: Mater Electron. 30 (2019) 18405–18412. https://doi.org/10.1007/s10854-019-02194-z.

[50] S. Shanmuga Sundari, R. Dhanasekaran, Influence of transition metal ions on multiferroic properties of lead-free NBT-BT ceramics, J. Adv. Dielectr. (2020). https://doi.org/10.1142/S2010135X19500450.

[51] B.H. Park, B.S. Kang, S.D. Bu, T.W. Noh, J. Lee, W. Jo, Lanthanum-substituted bismuth titanate for use in non-volatile memories, Nature. 401 (1999) 682–684. https://doi.org/10.1038/44352.

[52] Y. Noguchi, I. Miwa, Y. Goshima, M. Miyayama, Defect control for large remanent polarization in bismuth titanate ferroelectrics - doping effect of higher-valent cations, Jpn. J. Appl. Phys. 39 (2000) L1259–L1262. https://doi.org/10.1143/jjap.39.l1259.

[53] Y. Noguchi, T. Matsumoto, M. Miyayama, Impact of defect control on the polarization properties in $Bi_4Ti_3O_{12}$ ferroelectric single crystals, Jpn. J. Appl. Phys. Part 2 - Letters 44 (2005) L570–L572. https://doi.org/10.1143/JJAP.44.L570.

[54] S.-E. Park, T.R. Shrout, Ultrahigh strain and piezoelectric behavior in relaxor based ferroelectric single crystals, J. Appl. Phys. 82 (1997) 1804–1811. https://doi.org/10.1063/1.365983.

[55] S.-T. Zhang, A.B. Kounga, E. Aulbach, H. Ehrenberg, J. Rödel, Giant strain in lead-free piezoceramics $Bi_{0.5}Na_{0.5}TiO_3$ -$BaTiO_3$ - $K_{0.5}Na_{0.5}NbO_3$ system, Appl. Phys. Lett. 91 (2007). https://doi.org/10.1063/1.2783200.

[56] R. McQuade, T. Rowe, A. Manjón-Sanz, L. de la Puente, M.R. Dolgos, An investigation into group 13 (Al, Ga, In) substituted $(Na_{0.5}Bi_{0.5})TiO_3$-$BaTiO_3$ (NBT-BT) lead-free piezoelectrics, J. Alloy. Compd. 762 (2018) 378–388. https://doi.org/10.1016/j.jallcom.2018.04.329.

		process	Density (g/cm^3)	Relative density (%) (Typical error ± 0.5%)
S1	Calcination	850°C/10h	5,870 ± 0,001	98,6
		950°C/10h	5,860 ± 0,009	98,5
		1050°C/10h	5,943 ± 0,001	99,8
	Annealing	850°C/1h	5,960 ± 0,003	100
		950°C/1h	5,932 ± 0,001	99,7
		1050°C/1h	5,864 ± 0,001	98,5
S2	Calcination	850°C/10h	5,671 ± 0,001	95,3
		950°C/10h	5,660 ± 0,001	95,1
		1050°C/10h	5,667 ± 0,001	95,2
	Annealing	850°C/1h	5,765 ± 0,003	96,9
		950°C/1h	5,745 ± 0,001	96,6
		1050°C/1h	5,719 ± 0,002	96,1

Table 1: Densities of the powders elaborated by S1 and S2 routes after calcination and annealing. The relative densities were calculated with a reference value of 5.95 ± 0.01 g/cm^3 (reference file: PDF4 00-063-0299)

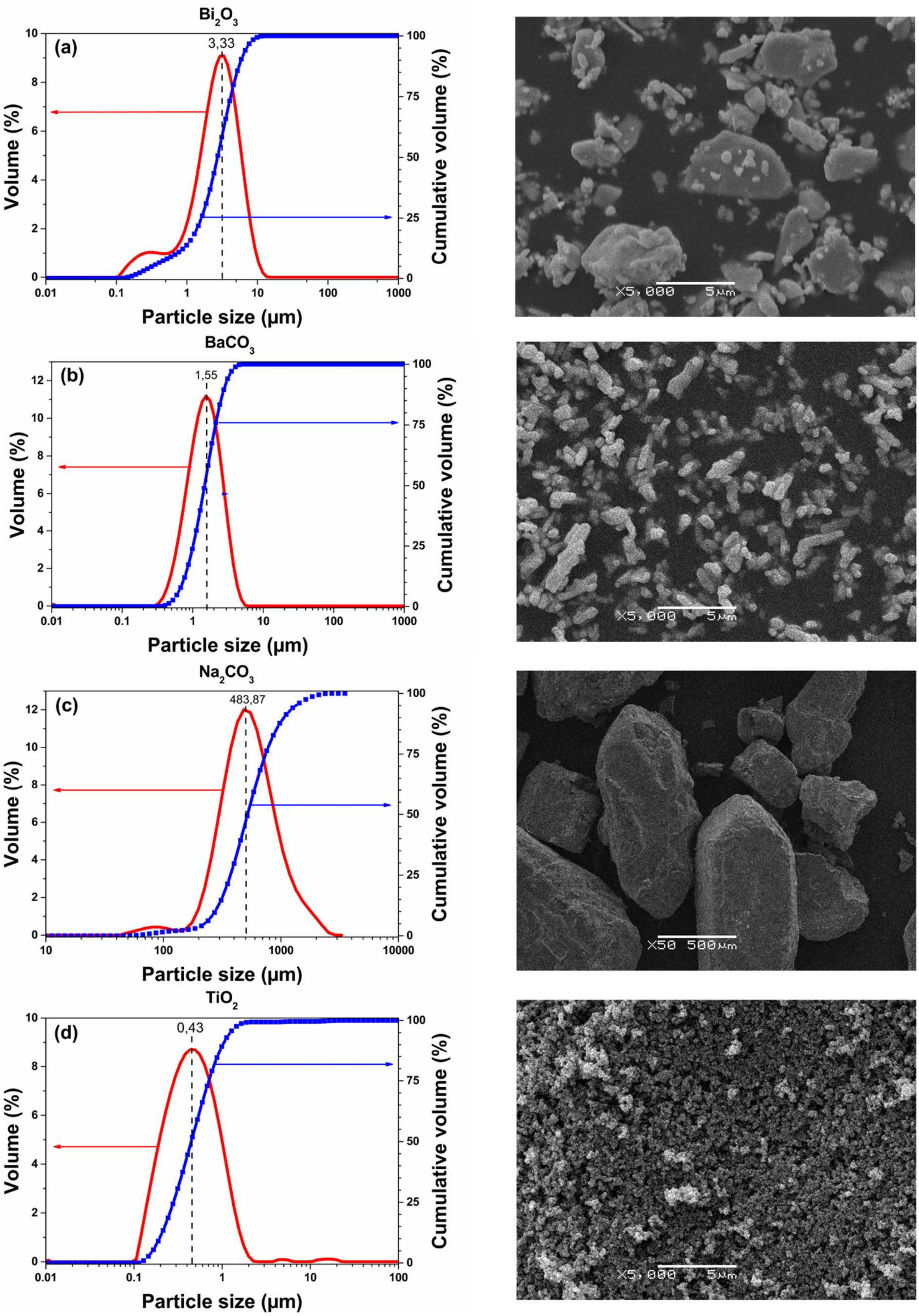

Fig. 1 : Particle size distribution and SEM pictures of a) Bi_2O_3, b) $BaCO_3$ c) Na_2CO_3 and d) TiO_2 (color online)

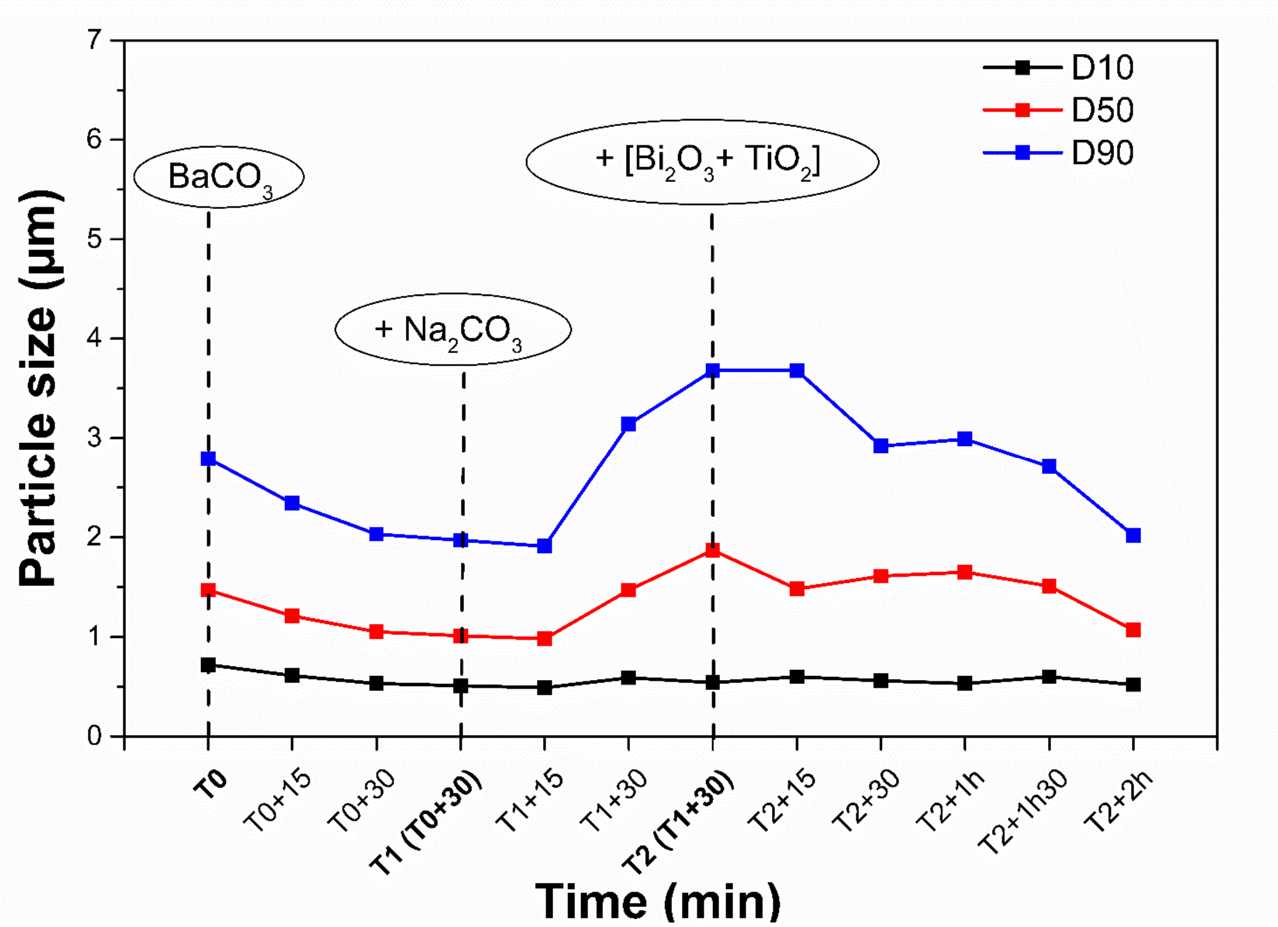

Fig. 2: Evolution of grain size distribution during S1 route attrition milling process. T0, T1 and T2 are the times of introduction into the mix of respectively $BaCO_3$, Na_2CO_3 and $[Bi_2O_3+TiO_2]$ (color online)

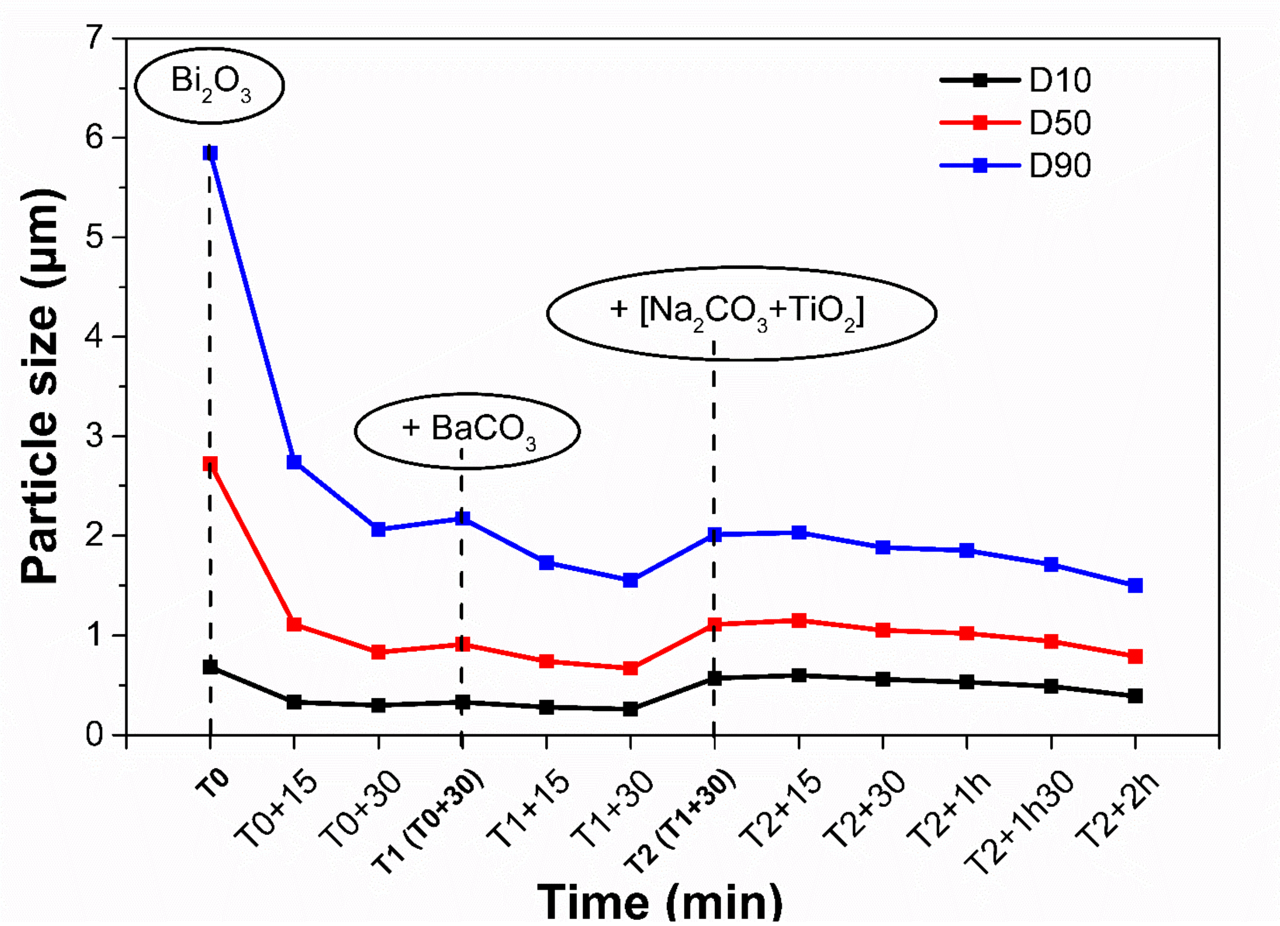

Fig. 3 : Evolution of grain size distribution during S2 route attrition milling process. T0, T1 and T2 are the times of introduction into the mix of respectively Bi_2O_3, $BaCO_3$ and [Na_2CO_3 + TiO_2] (color online)

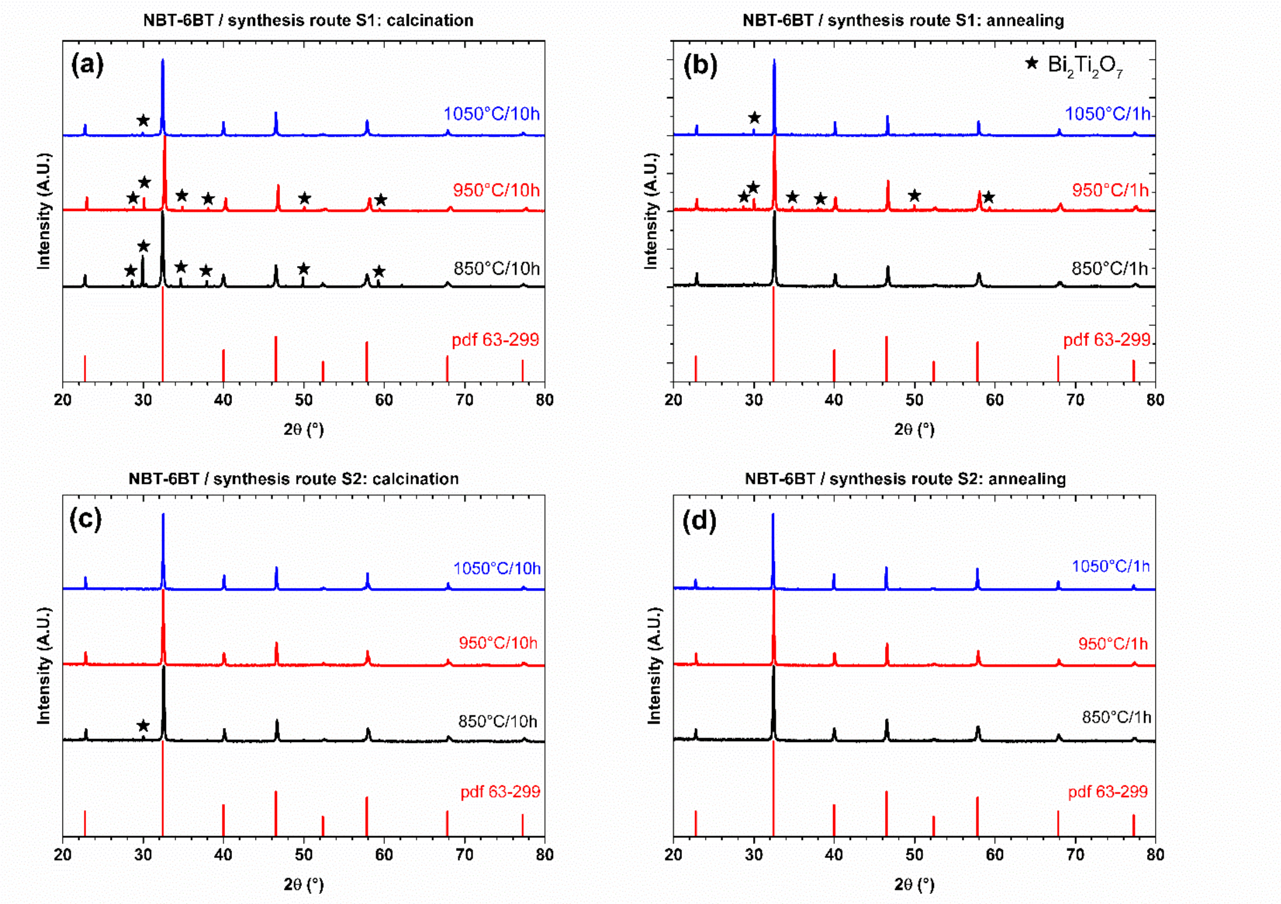

Fig. 4 : XRD patterns of the powders coming from: (a) S1 route after calcination, (b) S1 route after annealing, (c) S2 route after calcination and (d) S2 route after annealing (XRD patterns are normalized to unity using the main pic of NBT-6BT) (color online)

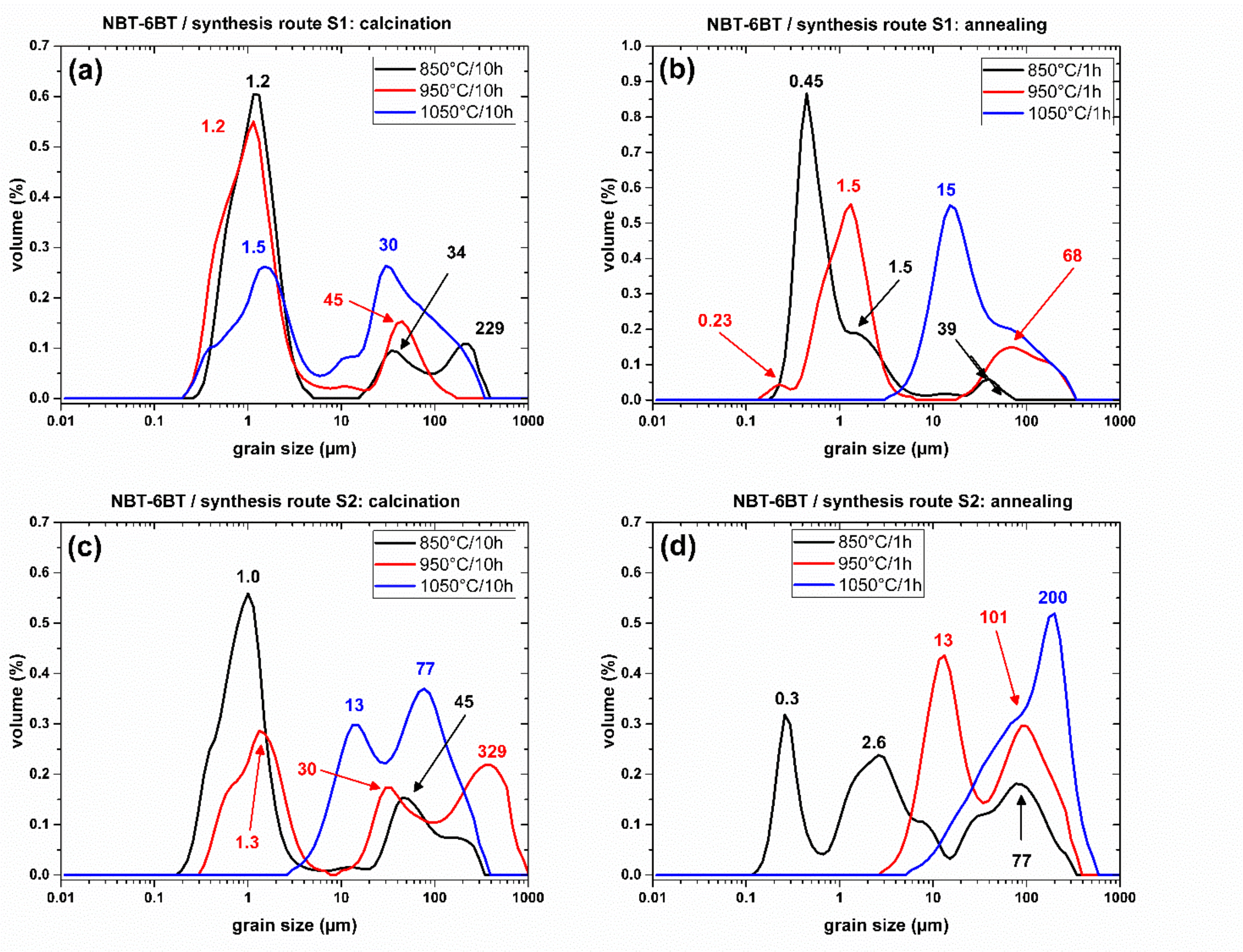

Fig. 5 : Grain size distribution of NBT-6BT powders coming from: (a) S1 route after calcination, (b) S1 route after annealing, (c) S2 route after calcination and (d) S2 route after annealing (color online)

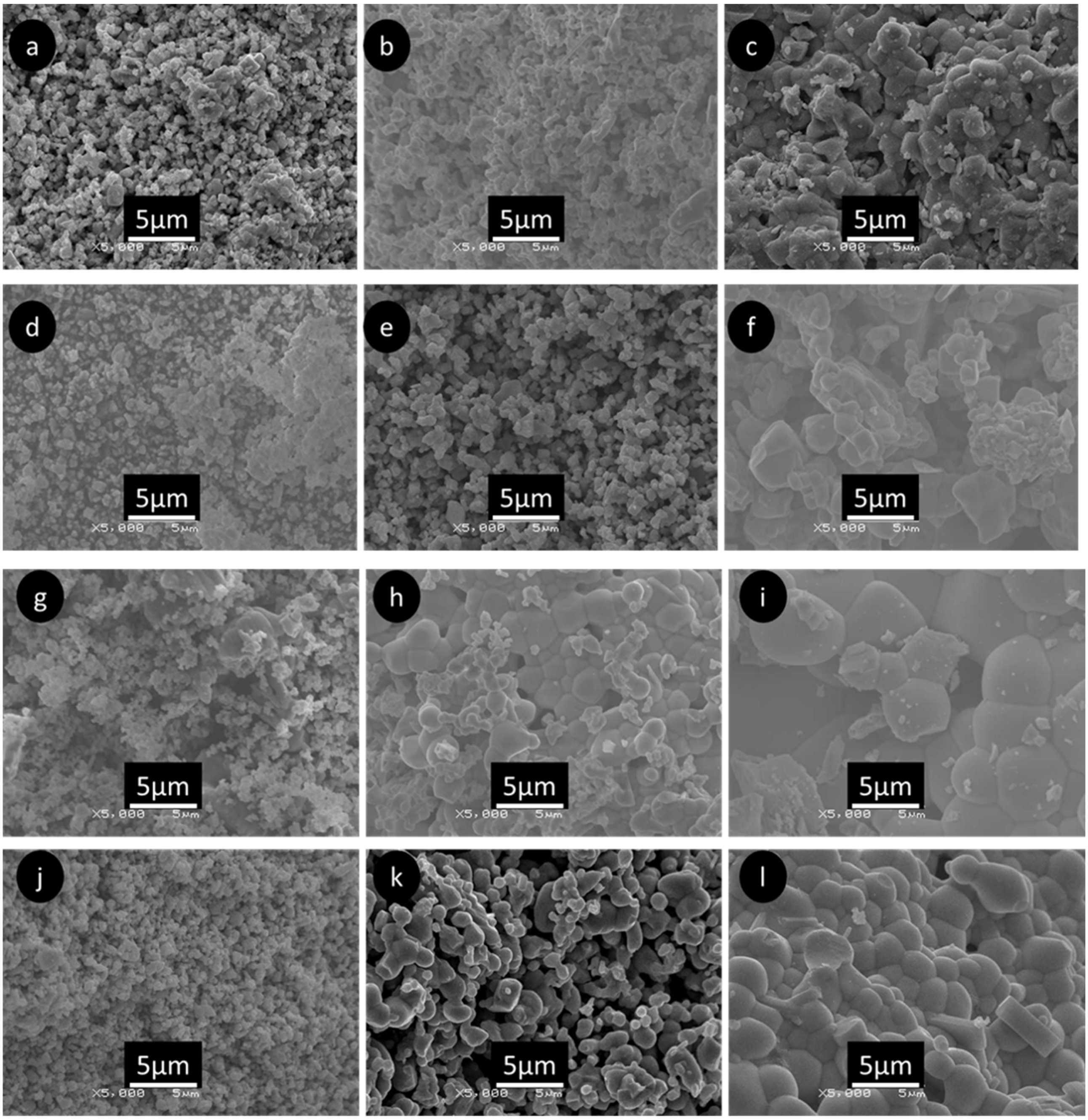

Fig. 6 : SEM pictures of the NBT-6BT powders coming from S1 route after calcination: (a) 850°C/10h, (b) 950°C/10h, (c) 1050°C/10h, S1 route after annealing (d) 850°C/1h, (e) 950°C/1h, (f) 1050°C/1h, S2 route after calcination; (g) 850°C/10h, (h) 950°C/10h, (i) 1050°C/10h, S2 route after annealing (j) 850°C/1h, (k) 950°C/1h, (l) 1050°C/1h

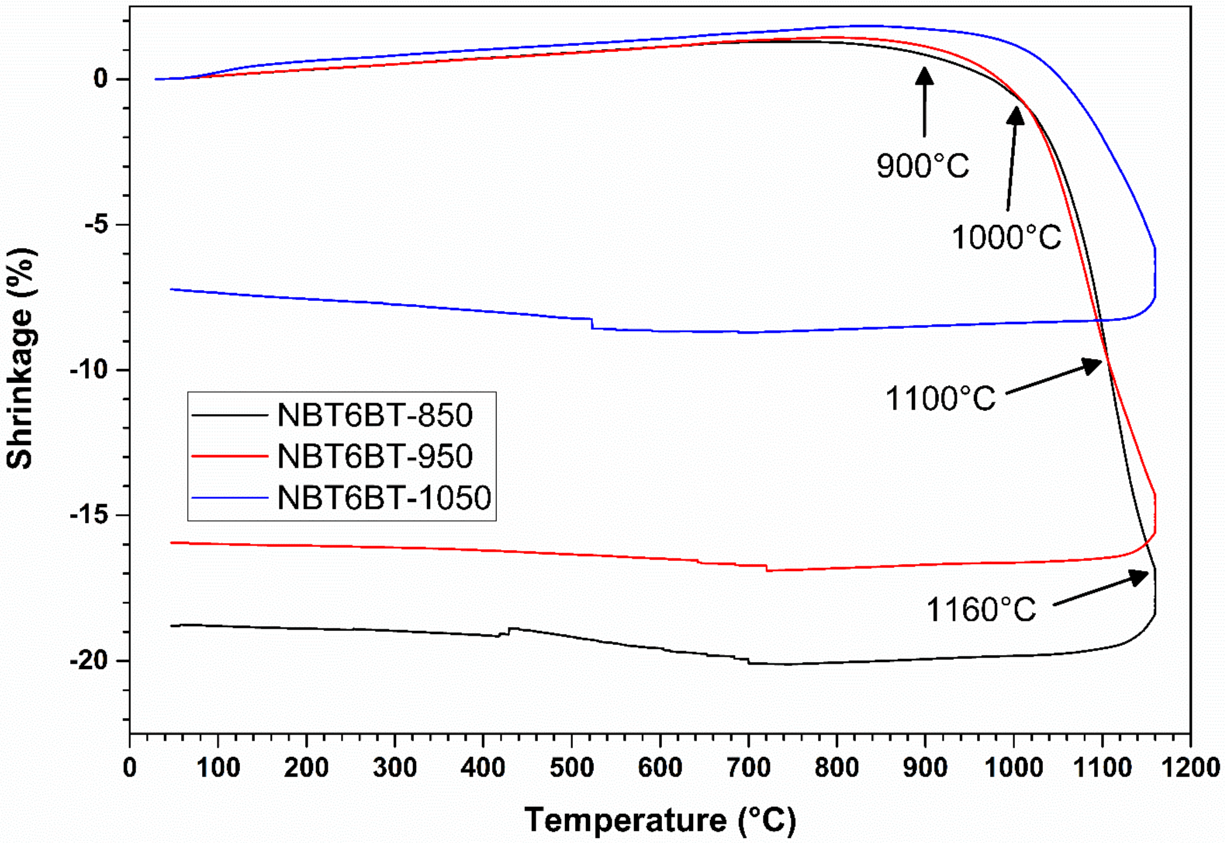

Fig. 7: Dilatometric study of the powders coming from S2 route (color online)

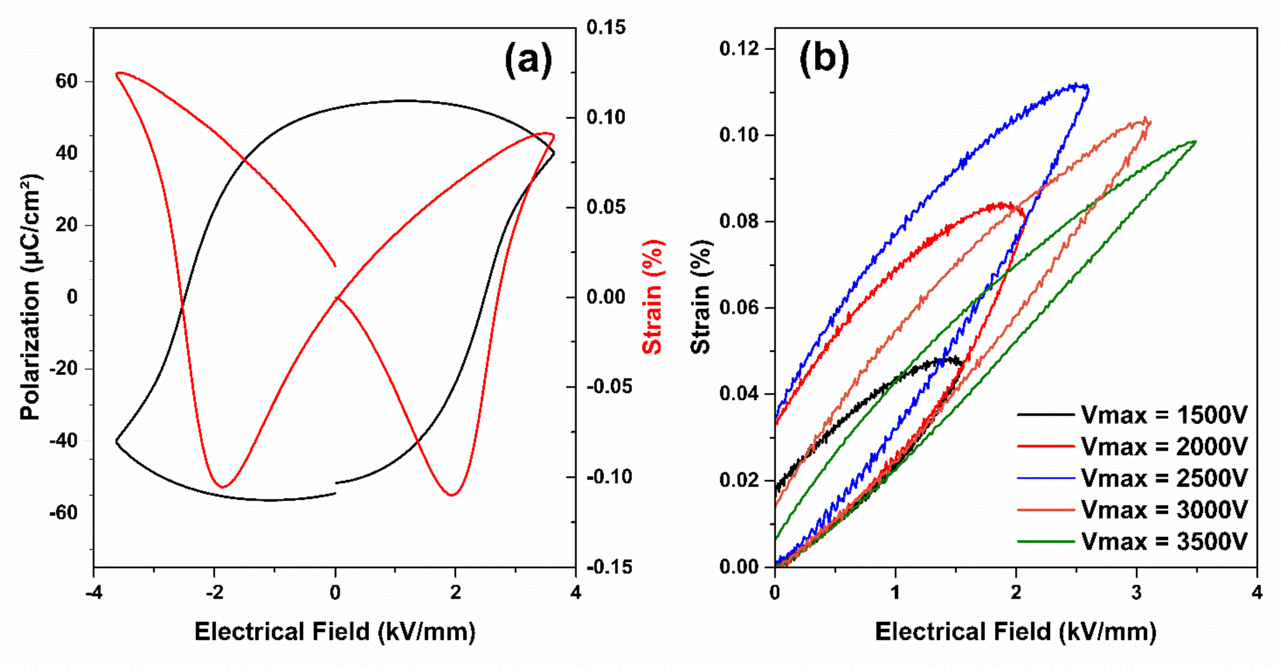

Figure 8 : (a) P(E) and strain hysteresis cycles and (b) unipolar strain cycle for different values of maximum voltage for NBT-6BT poled sample sintered at 1150°C for 10h (color online)

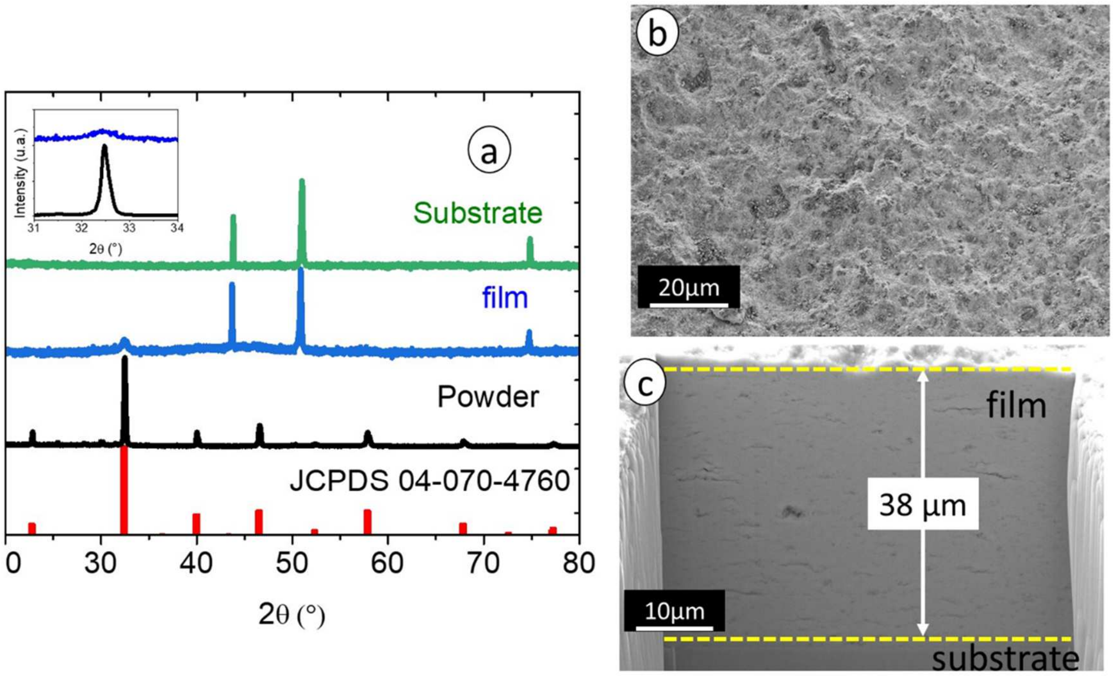

Figure 9 : (a) XRD patterns for kovar substrate, NBT-6BT powder and NBT-6BT film obtained by AD, (b) SEM top view and (c) SEM cross section of the NBT-6BT AD film